Instrument: **SP1 Cooperation**

Thematic Priority: **Priority Area 1.1.6.3 "Global Change and Ecosystems"**

FP7 Collaborative Project – Grant Agreement 212492

CLARIS LPB
A Europe-South America Network for Climate Change Assessment and Impact Studies in La Plata Basin

DELIVERABLES

D9.15: Prediction of climate change scenarios effects on the Parana delta front growth and the consequences on the available area extension to Buenos Aires urbanization assessed

Due date of deliverable: Month 42

Start date of project: **01/10/2008** Duration: **4 years**

Organization name of lead contractor for this deliverable: National Institute for Water (INA)

Deliverable No	Deliverable title	WP	Lead beneficiary	Estimated indicative person-months (permanent staff)	Nature	Dissemination level	Delivery date
D9.15	Prediction of climate change scenarios effects on the Parana delta front growth and the consequences on the available area extension to Buenos Aires urbanization assessed	9	P16-INA	***	R	CO	42

Leandro D. Kazimierski, Nicolás D. Badano, Martin Sabarots Gerbec, Mariano Re, Martín Irigoyen, Pablo Spalletti, Angel N. Menéndez and José D. Brea

Hydraulic Laboratory, National Institute for Water (INA), Ezeiza, Argentina

Introduction

The Parana River is one of the largest rivers in South America. Due to its enormous basin (2.5 million km^2), it has a modulus discharge of 17,000 m^3/s, with a total sediment load of 160 million ton/year. Upon discharging to the estuarine waters of the Plata River, which divide Argentina and Uruguay, the Parana River Delta is formed (Figure 1). It currently has approximately 320 km of length, with a maximum width of 60 km.

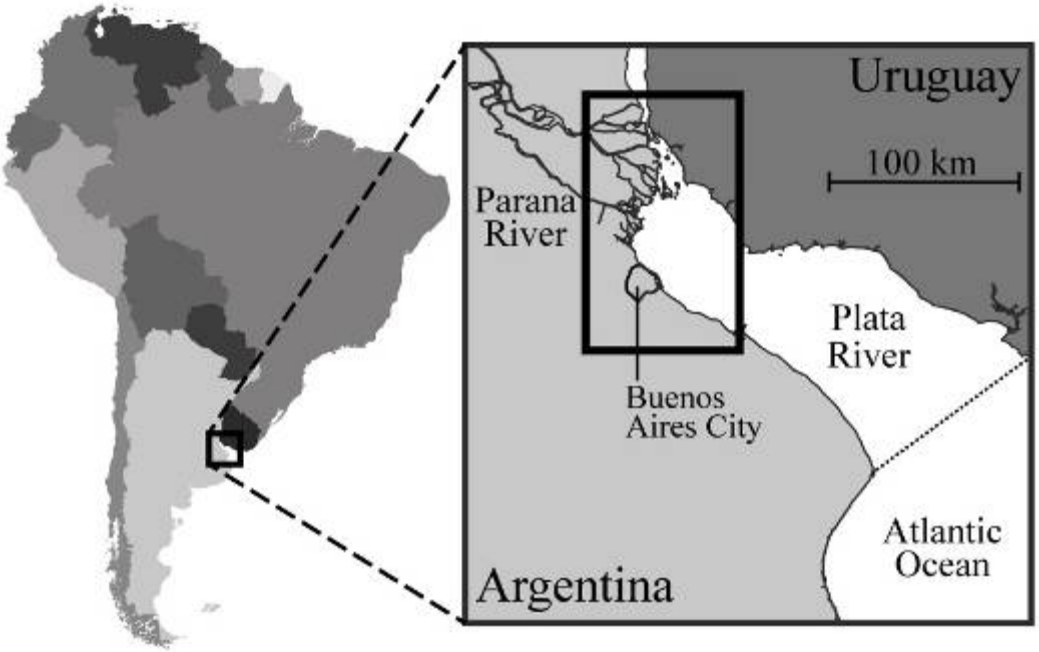

Figure 1. Parana River Delta location.

The Parana River Delta (close to Buenos Aires, Argentina) shows a continuous growth. The rate of advancement of the Delta Front reaches several tens of meters per year in the most active zones, along its 60 km frontline. This process has significant economic consequences. In the context of Climate Change,

projections on its future trends constitute important information that may help for land use management and planning. Mathematical modeling of the Delta Front advancement, validated using recent satellite imagery and cartographic data, is proposed as an appropriate tool for assessing future trends of the system evolution under various scenarios. Improving upon previously published modeling studies, the current methodology is based on the hydrodynamic modeling of the frontal area, solving the shallow water equations, and a coupled transport model for suspended sediments, which includes advection, diffusion, deposition and resuspension. The bottom and coastal morphology changes are also accounted for in a coupled fashion. The hydrodynamic model is validated through comparison between calculated and measured currents. The validation of the hydro-sedimentologic-morphologic model, as a whole, is performed by comparing the simulated and observed front advancement for the 1994-2007 period. Future scenarios related to Climate Change are evaluated, including variations in the hydrodynamics conditions (mean sea level) and sediment yield.

In a context where most of the world's mayor deltas are at risk (Syvitski et al., 2009), the Parana River Delta has shown continuous growth during recorded history till present day. Historical cartographic data allows reconstructing the Delta Front advancement since the 1700s (Figure 2). Two main sub-fronts are observed: Northern with a present mean advancement rate of 27 m/year, complemented by a continuous enlargement of downstream islands; and Southern with 72 m/year.

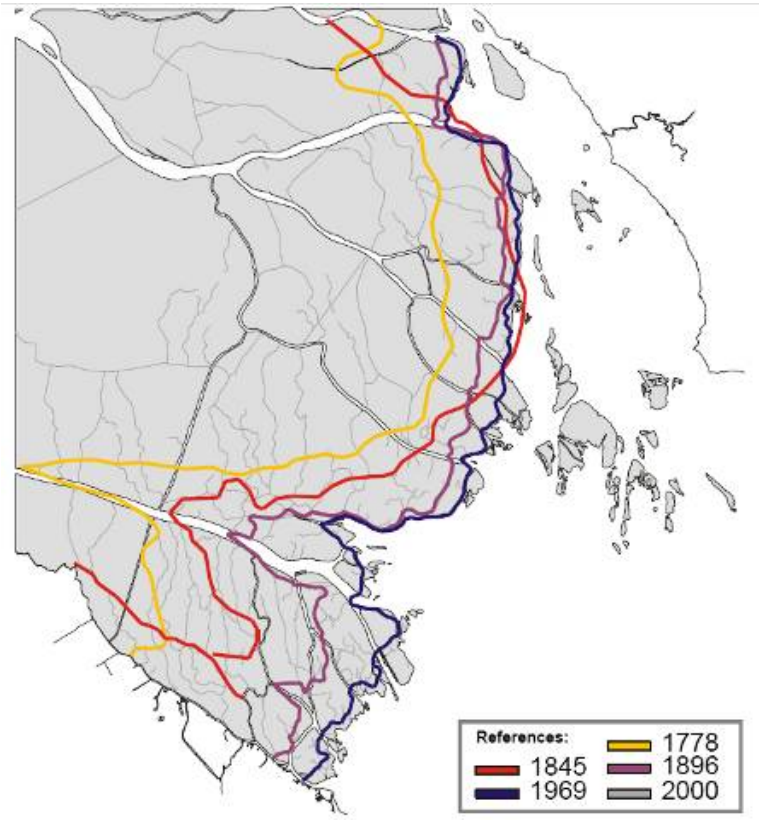

Figure 2. Historical advance of the Parana River Delta Front (Sarubbi, 2007).

The delta growth has significant economic consequences. It not only has influence over potential productive activities within the delta, but Buenos Aires city itself is in close proximity to the delta front (11 km), with the outskirts of its metropolitan area extending to the very front (Figure 3).

Figure 3. Paraná Delta Front (subfront Paraná de las Palmas) and urban zones.

The growth of the delta is produced by the deposition of fine sands and coarse silts, carried from the northwestern part of the Upper Parana basin, accounting for approximately 15% of the total sediment load of the river, 24 million ton/year (Sarubbi, 2007). The northwestern part of the Plata Upper basin includes zones of northern Chile, southwestern Bolivia and northwestern Argentina. This region is characterized by the Andes, with altitudes above 4000 m (*Altiplano*) decreasing to 200 m to the east. Zones of little vegetation with significant slopes and average annual rainfall below 500 mm are vulnerable to soil erosion. Rivers and creeks of this zone transport the eroded material to the east to be conducted by the two main rivers in the region: Bermejo and Pilcomayo River (Figure 4).

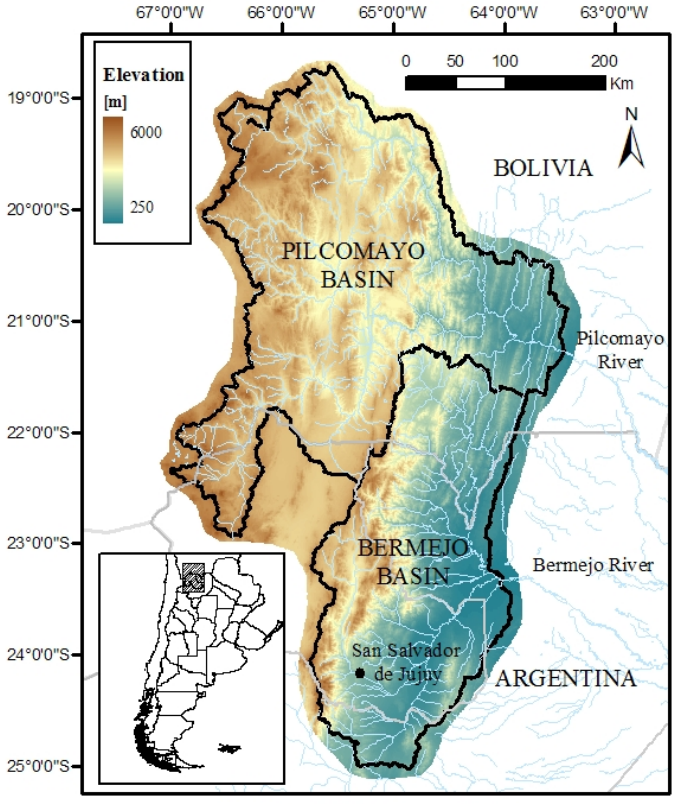

Figure 4. Pilcomayo and Bermejo River Basin.

In the context of Climate Change, projections on its future trends constitute important information that may help the management and planning for the region. Furthermore, sediment load projections from Bermejo River will allow projections in Parana Delta Front advancement.

Sediment yield from the Upper Plata basin

It is important to determine the sediment yield from the Upper La Plata Basin due to the magnitude of the load transported by the main rivers of this region. Previous work (Alarcon et *al*., 2003; Amsler and Drago, 2007; among others) clearly demonstrated the dominant role of the Bermejo River in the wash load supply the Paraná River, downstream of the confluence with the Paraguay River and the much smaller contribution of wash load from the Alto Paraná (exacerbated by the retention effect of Brazilian dams) (Re et *al*., 2009). Considered one of the rivers with higher production rate and sediment transport in the world, the Pilcomayo River presents a complex sedimentological and morphological behavior, which is its distinctive natural feature in the region, which has not yet been solved by the state art in the field (Brea and Spalletti, 2011).

The Gavrilovic method was applied for analyzing erosional processes in the Upper Plata basin (Bermejo and Pilcomayo basins). Since an array of empirical coefficients based on the physical characteristics of the basins is used in the method, we describe GIS based techniques for data preparation and modeling.

The present and future scenarios (Climate Change scenarios) of sediment yield were studied in this work. For future scenarios were varied conditions of precipitation and temperature held constant the land use parameters.

In order to analyze the impact of Climate Change in the Bermejo and Pilcomayo basins (Upper Plata basin) four Regional Climatic Models (RCM) were used. These regional models have boundary conditions from three Global Climatic Models (GCM). The combinations of them result in seven scenarios. Five of them have the 1960-2100 complete series (Complete) and the remaining two have periods of 30 years (Partial): 1961-1990 (present scenario), 2011-2040 (near future), 2041-2070 (intermediate future) and 2071-2100 (far future) (Table 1).

Table 1. Combination of RCM and GCM.

RCM	GCM		
	HadCM3-Q0	EC5OM-R3	IPSL
RCA	Complete (3)		
RegCM3	Partial		
PROMES	Complete		
LMDZ		Partial	Complete

Erosion Potential Method - Gavrilovic methodology

The *Gavrilovic Method* is a model for qualifying the erosion severity and estimating the total annual sediment yield of a catchment area. This model was initially developed by Gavrilovic (1988), and was applied in balcanic, alpine and latin-american basins (Peviani et *al.*, 1994; Brea et *al.*, 1999; and Globevnik, et *al.*, 2003; among others). *Gavrilovic Method* is parametric distributed model and considers six factors such as; surface geology and soils, topographic features, climate (including mean annual rainfall and mean annual temperature) and land use. This empirical method allows calculate the sediment volume yield by erosion and transported to the end of the basin (G) as the product of the mean annual sediment yield by surface erosion (W) and the sediment retention coefficient (R).

$$G = W \cdot R \quad [m^3/year] \qquad [1]$$

The expression for determining the mean annual sediment yield by surface erosion is:

$$W = T \cdot h \cdot \pi \cdot z^{3/2} \cdot F \quad \left[m^3/year\right] \qquad [2]$$

with T (temperature coefficient) obtained by $T=[(t/10)+0,1]^{1/2}$ and z (erosion coefficient) by $z=X*Y*(\varphi+I^{1/2})$, where t is the mean annual temperature [°C], h the mean annual precipitation [mm/year], F the basin surface [km²], X the land use coefficient, Y the coefficient of rock and soil

resistance to erosion, φ the coefficient value for the observed erosion process, and I the average slope of the basin [%].

The retention coefficient R indicates the ratio of the volume of sediment at the end of the basin and the total volume of material produced by surface erosion. Its value depends on parameters that characterize the basin and its calculation is this formula (Zemlijc, 1971):

$$R = \frac{(O \cdot D)^{1/2} \cdot (L + L_i)}{(L + 10) \cdot F} \qquad [5]$$

where O is the perimeter [km], D is the difference in average level in the basin [km], Li is the total length of lateral river tributaries [km], L is the length of the basin by the main channel talweg [km], and F the basin area [km^2].

Data preparation and model calibration

When the drainage basin is not uniform with respect to the erosion coefficients, Gavrilovic suggested that the basin should be divided into smaller sub areas (hydrographic units).

The coefficients based on physical features of the basins (X, Y, φ, J, and R), were estimated using available data base from Bolivia and Argentina, calculation algorithms, and expertise of the authors as a product of more than 20 years of experience in the field (Spalletti and Brea, 2006).

Pilcomayo and Bermejo Upper Basins were subdivided in approximately 700 sub-basins. For each one, those coefficients were indicated. All the data maps were implemented in a GIS (Geographical Information System).

The coefficients X, Y, and φ, respectively, represent the degree of soil protection provided by vegetation and human intervention, the degree of soil erodibility, and the state of instability of the basin.

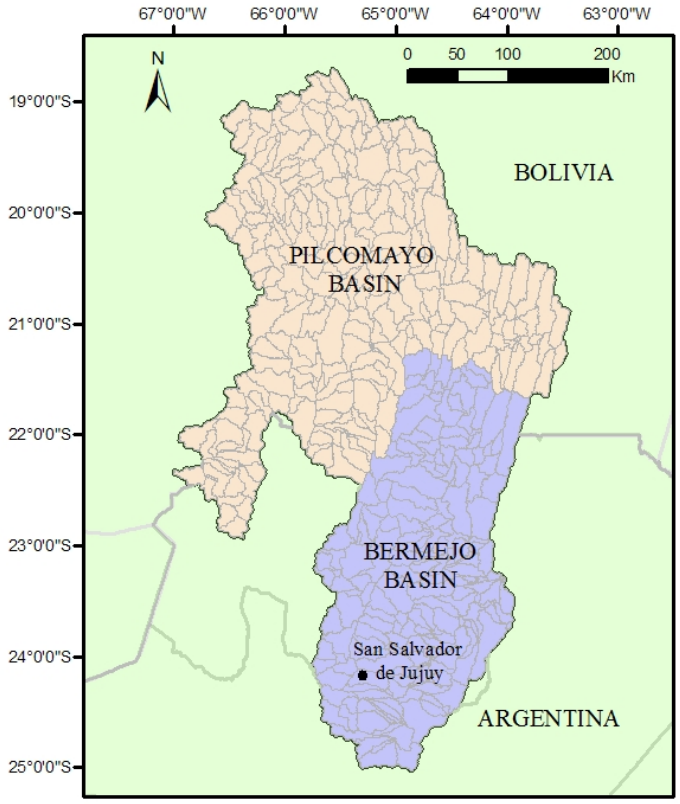

Figure 2. Sub-basins.

The degree of soil protection provided by vegetation and human intervention (X) takes values between 0.05 and 1, in terms of the land use and the vegetal coverage. The map of the X variable was developed with the RGB 752 bands of LANDSAT 5 satellite images (Irigoyen et *al*., 2011). The degree of soil erodibility (Y) takes values between 0.25 and 2 depending on the type of surface soil.

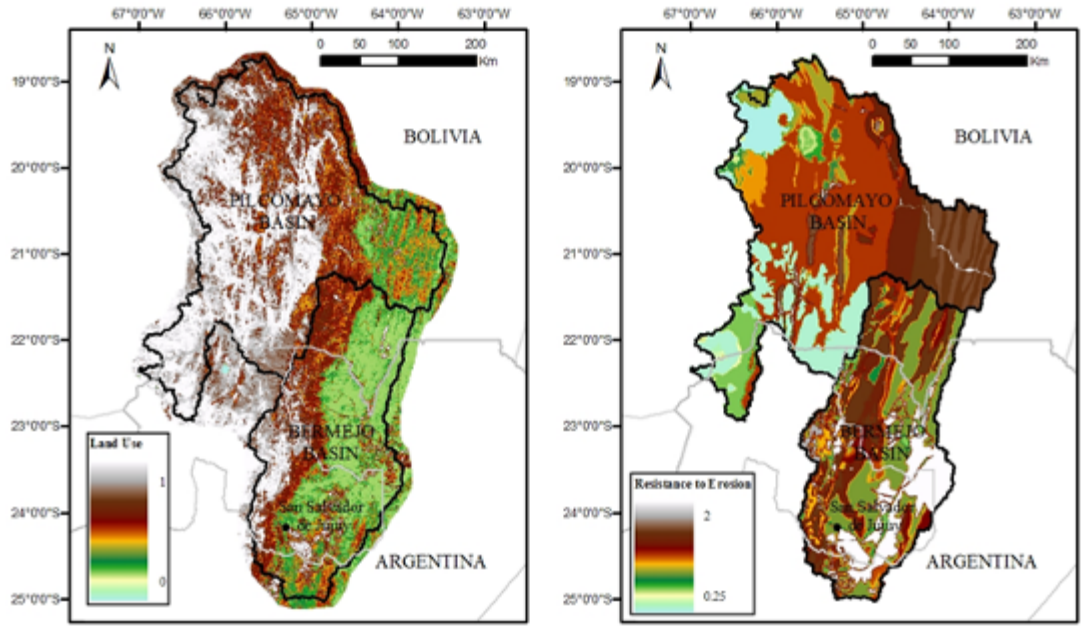

Figure 3. Land Use Coefficient (X) and Coefficent of Rock and Soil Resistance to Erosion (Y)

The coefficient of the observed erosion process (φ) takes values between 0.1 and 1, according to the types of erosion observed, the percentage of the basin affected and its severity. The gradient of the slope surface - I - was obtained with SRTM (*Shuttle Radar Topographic Mission*) images (downloaded from: http://srtm.csi.cgiar.org).

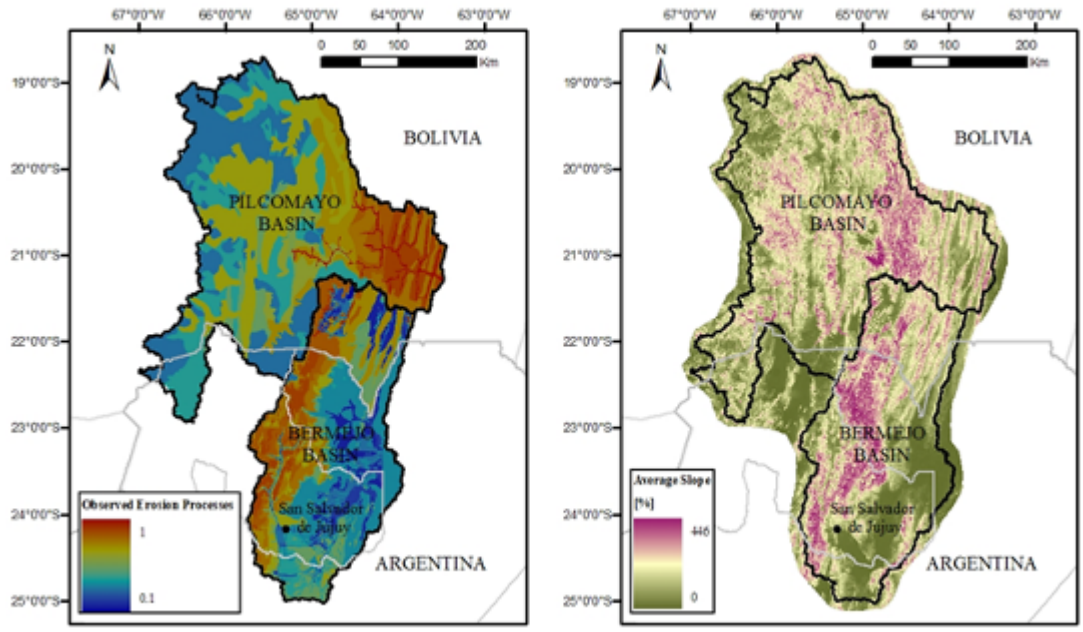

Figure 4. Coefficient value for the observed erosion processes (ϕ) and Average Slope (J)

The climate of the region is governed by the South America Monsoon System (Vera et *al*, 2006) with a wet season centered on the moths of December to March and the rest of the year predominantly dry (Aceituno, 1996) except for the events generated by the cut-off lows explained by Campetella et *al* (2009) being more frequent in austral autumn followed by winter, spring and summer. The summer rainfall in Bermejo Basin depends mainly of the Pacific and Indian Ocean sea surface temperatures and explains 50% of the variance (Gonzales and Murgida, 2012). The Altiplano (Pilcomayo Basin) interannual rainfall anomalies can be explained by the generalized warming (cooling) of the tropical troposphere during the warm (cold) phase of ENSO, and the associated changes in the seasonal mean zonal flow aloft at tropical-subtropical latitudes (Garreaud and Aceituno, 2001). Aceituno (1996) mentions that the prevailing winds from the east at intermediate levels correlate with increased rainfall in the area of interest. The interaction between the moisture with the radiative heating, orographic forcing and synoptic systems (cold fronts) generate heavy rainfall mostly convective-type (high intensities for short periods of time).

Present climate for the region was represented by the mean fields of rainfall and temperature from the period 1961-1990 (Figure 5).

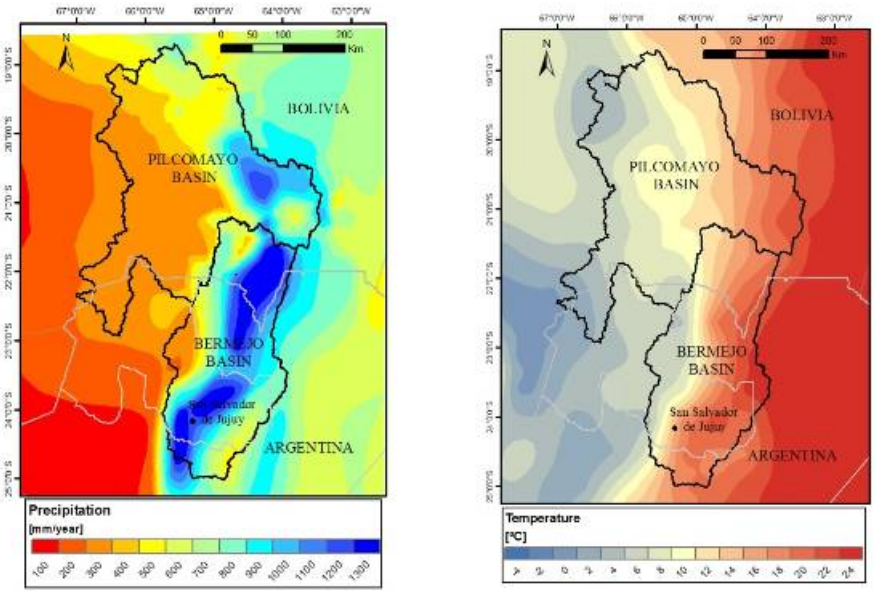

Figure 5. a) Mean Annual Precipitation b) Mean Annual Temperature.

The advantage of using RCMs than GCMs is the best discretization (Figure 6), which in areas with complex topography is essential when modeling the physical processes taking place in the atmosphere. Although the improvement is remarkable, there are still large differences between observed and simulated grids. Figures 7 and 8 compares the observed precipitation and temperature fields for present versus the results from different RCMs.

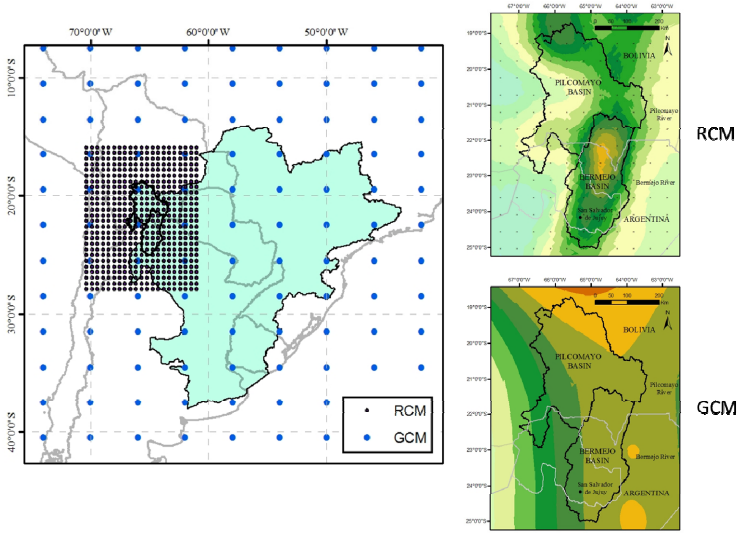

Figure 6. Comparison between RCM and GCM.

As it is observed in most of the models, the position of maximum rainfall at the basins is well located, although none correctly simulates its extension (Figure 7). The annual accumulated precipitation simulated in the area of maximum rainfall, except in the RegCM3 model, can be considered correct. It is important to detail, that the observed precipitation map was constructed with a very small database for the extension and the complex topography of the area, with major uncertainties in the high mountain area.

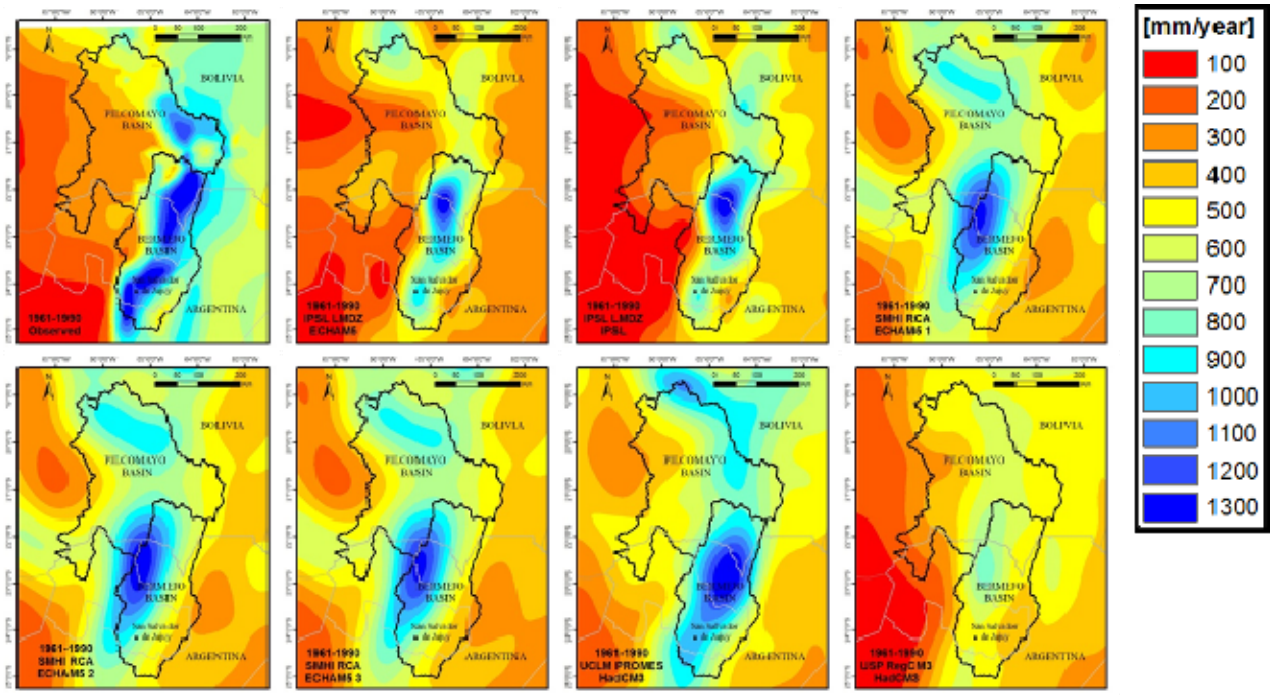

Figure 7. Precipitation fields for the seven models and 1961-1990 observed data.

Temperature fields (Figure 8) shows that models tend to generate a higher gradient in the mountain area compared with the map of observed data (considering also the lack of reliable information). Would not be surprising that models can see certain patterns of temperature fields not seen in the data (i.e. northwest of Pilcomayo basin).

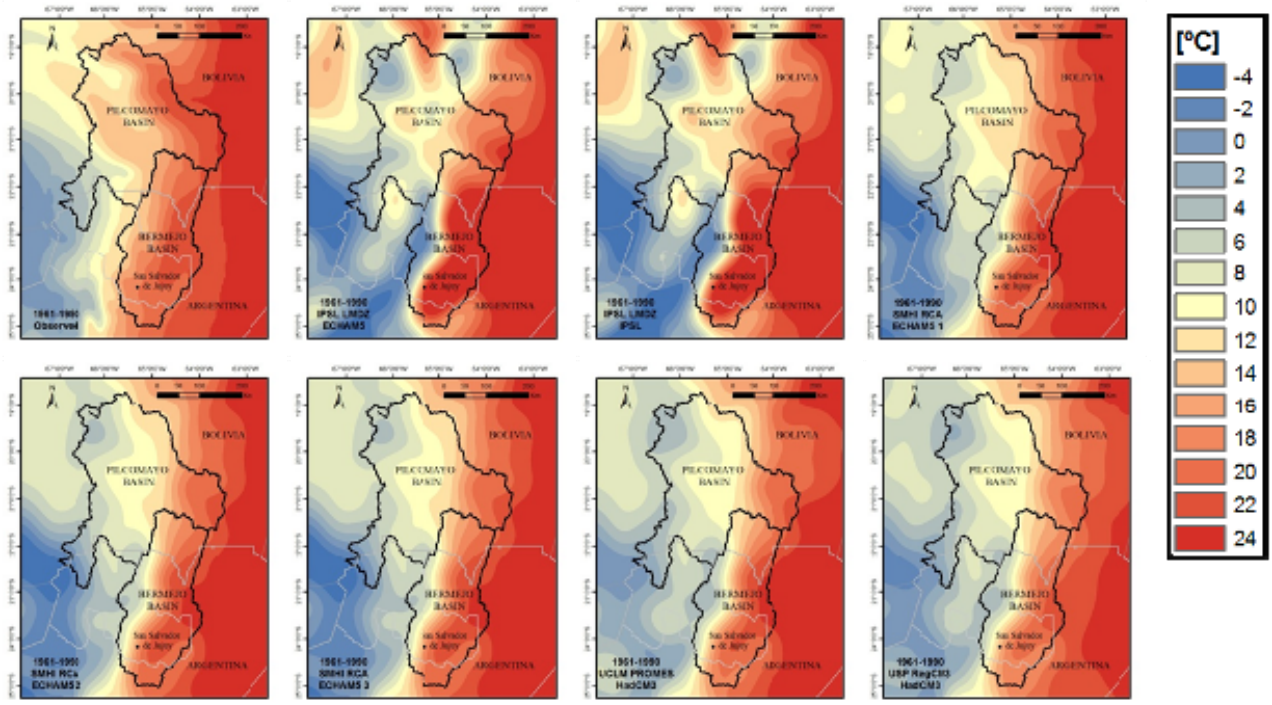

Figure 8. Temperature fields for the seven models and 1961-1990 observed data.

As a validation for the base scenario (1961-1990) of this methodology, modeled results were contrasted with data from reservoir sedimentation of the study area and data from gauging stations where solid discharge information was available. Results demostrate the feasibility of using this methodology to evaluate the processes of sediment production by surface erosion in this kind of basins.

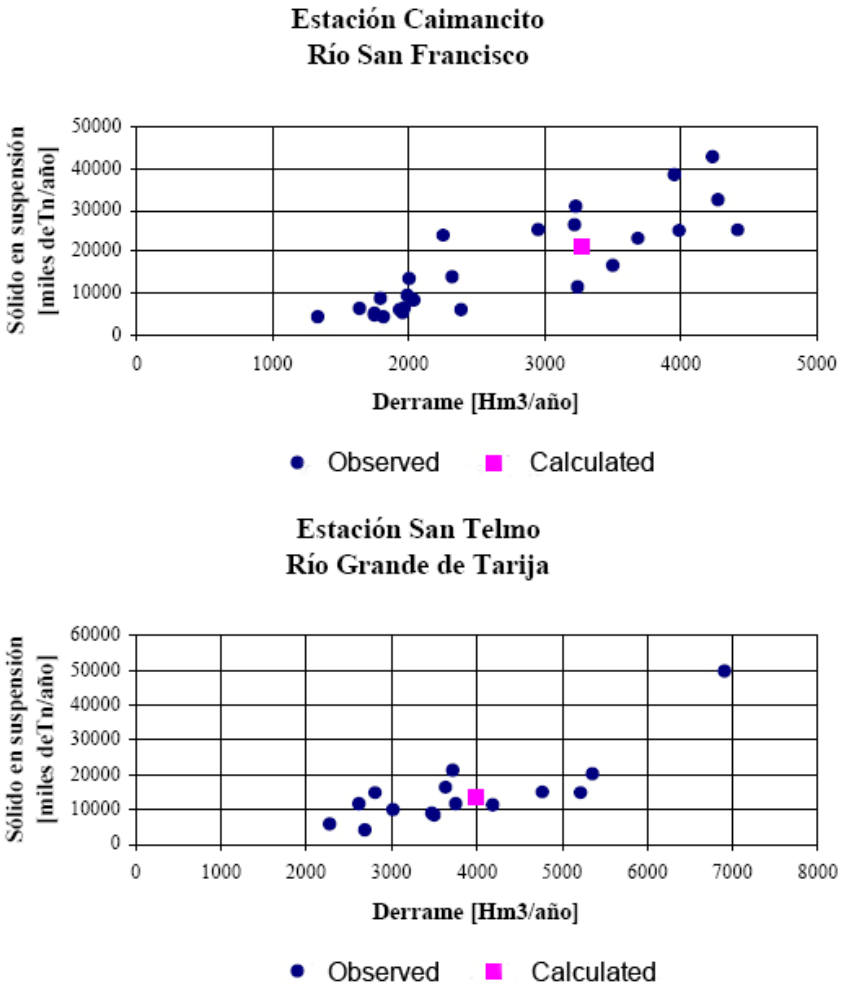

Figure 9. Calibration in two sub basins.

Future scenarios

Calculations for three future periods (2011-2040, 2041-2070 and 2071-2100) were made with data from the seven models. The exceptions of these calculations were: i) period 2041-2070, missing data for models IPSL_LMDZ_ ECHAM5 and UCM_RegCM3_HadCM3; ii) period 2071-2100, errors in the output of the model UCLM_PROMES_HadCM3. For calculating temperature variations from the present average, the following scheme was used for correcting BIAS:

$$T^{SIM} = \frac{T^{OBS}}{T^{SIM}_{Current}} T^{SIM}_{Scenario} \qquad [6]$$

Where T^{OBS} represents the mean observed temperature for the period 1961-1990, $T^{SIM}_{Current}$ is the temperature from each model for the period 1961-1990, $T^{SIM}_{Scenario}$ are the model result for future scenarios and T^{SIM} the map of temperatures to calculate the sediment yield.

The same scheme was used for the precipitation calculations:

$$P^{SIM} = \frac{P^{OBS}}{P^{SIM}_{Current}} P^{SIM}_{Scenario} \qquad [7]$$

Mean sediment yields were plotted for the considered periods for the different models (Figure 10). First, it was observed that for the near future the trend is to maintain current production, while in the intermediate future there is a slight trend in the Bermejo basin and a stronger trend in the Pilcomayo basin to decrease production. Finally, in the far future the trend is reversed and a majority of models indicate an increase in production in the Bermejo basin and maintenance of current levels in Pilcomayo basin. In far future scenarios the dispersion increases for both basins and in a similar way.

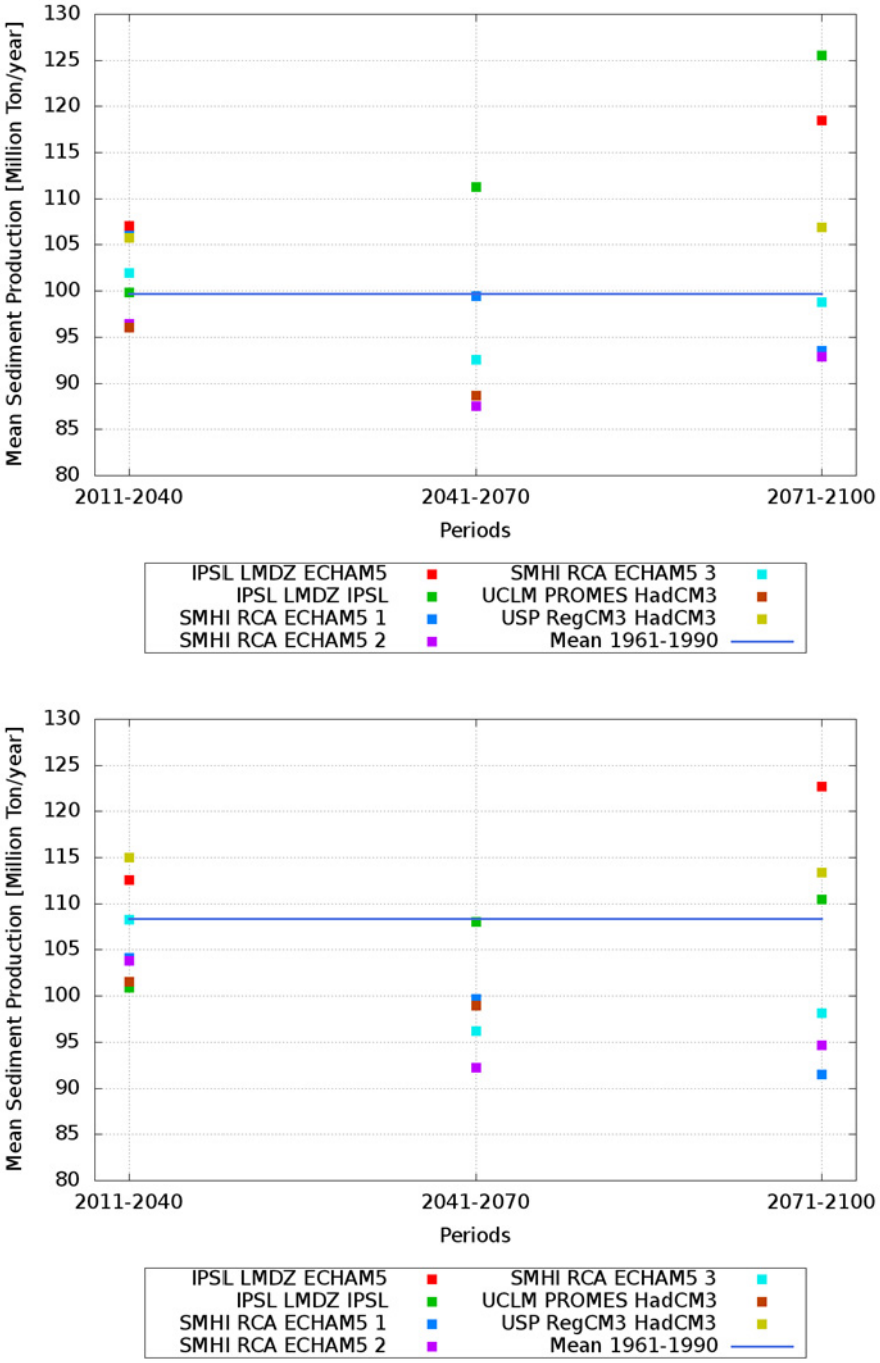

Figure 10. Mean sediment yield in, a) Bermejo Basin; b) Pilcomayo Basin.

With mean annual temperature and precipitation from five RCMs, time series on sediment production for each basin were performed with the five complete models (Figures 11 and 12).

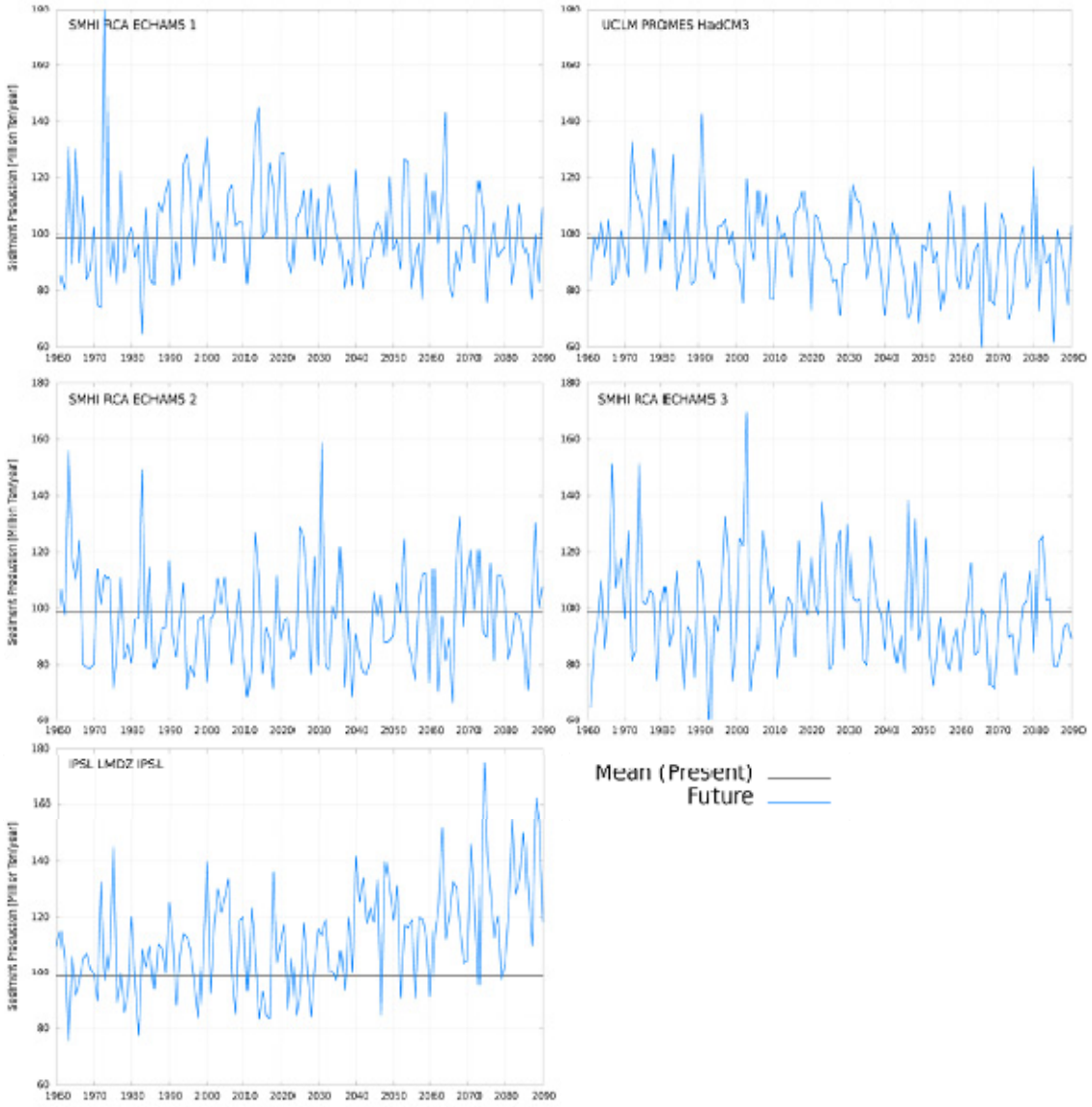

Figure 11. Annual series of sediment production -blue- in Bermejo basin and 1961-1990 mean -black-.

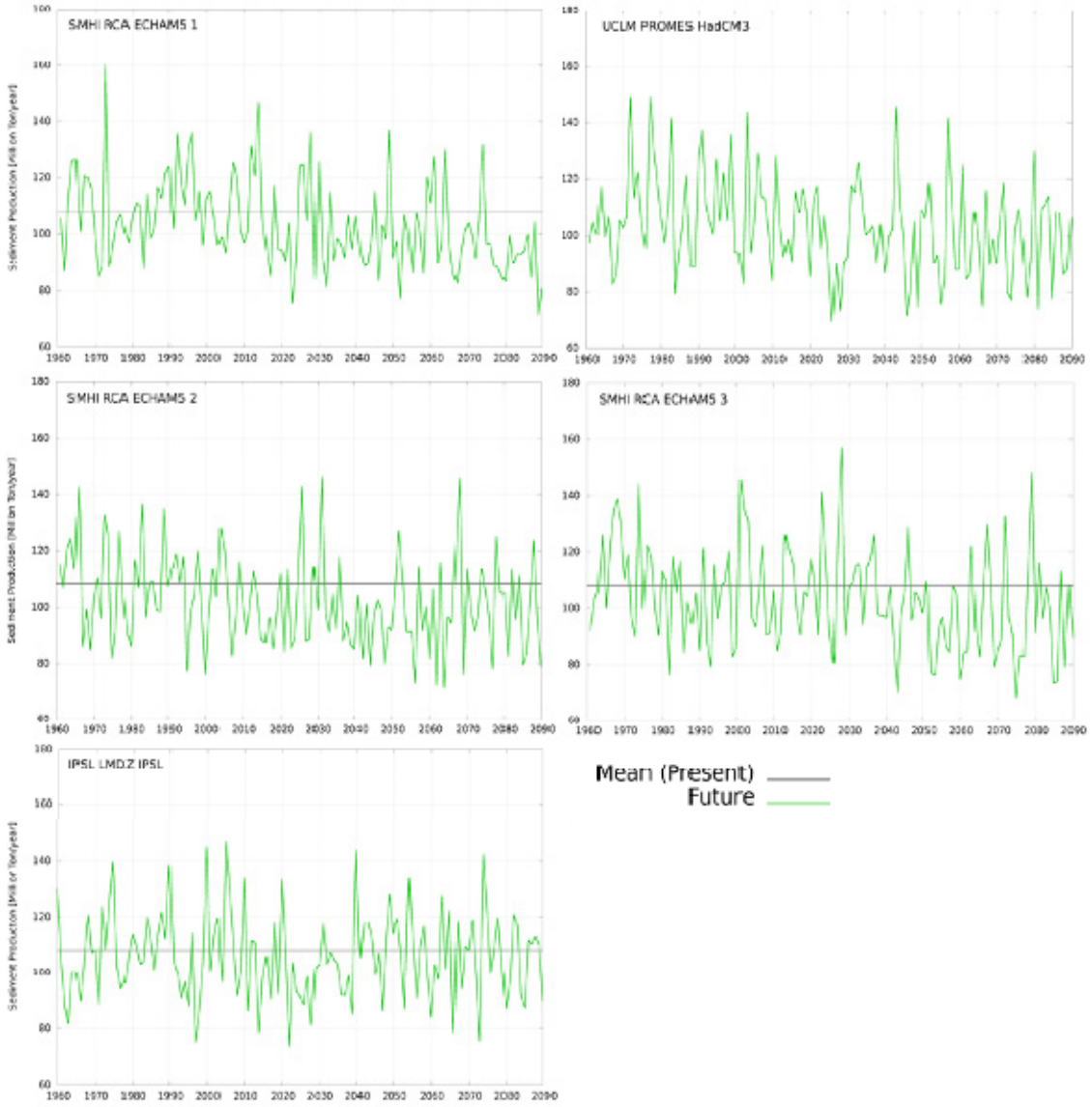

Figure 12. Annual series of sediment production -green- in Pilcomayo basin and 1961-1990 mean -black-.

It was observed that there is a strong correlation between annual rainfall and the rate of annual sediment generation for the Pilcomayo River basin (Figure 13a). In the case of the Bermejo River basin (Figure 13b) there is a greater dispersion, mainly attributable to variations in the spatial distribution of precipitation.

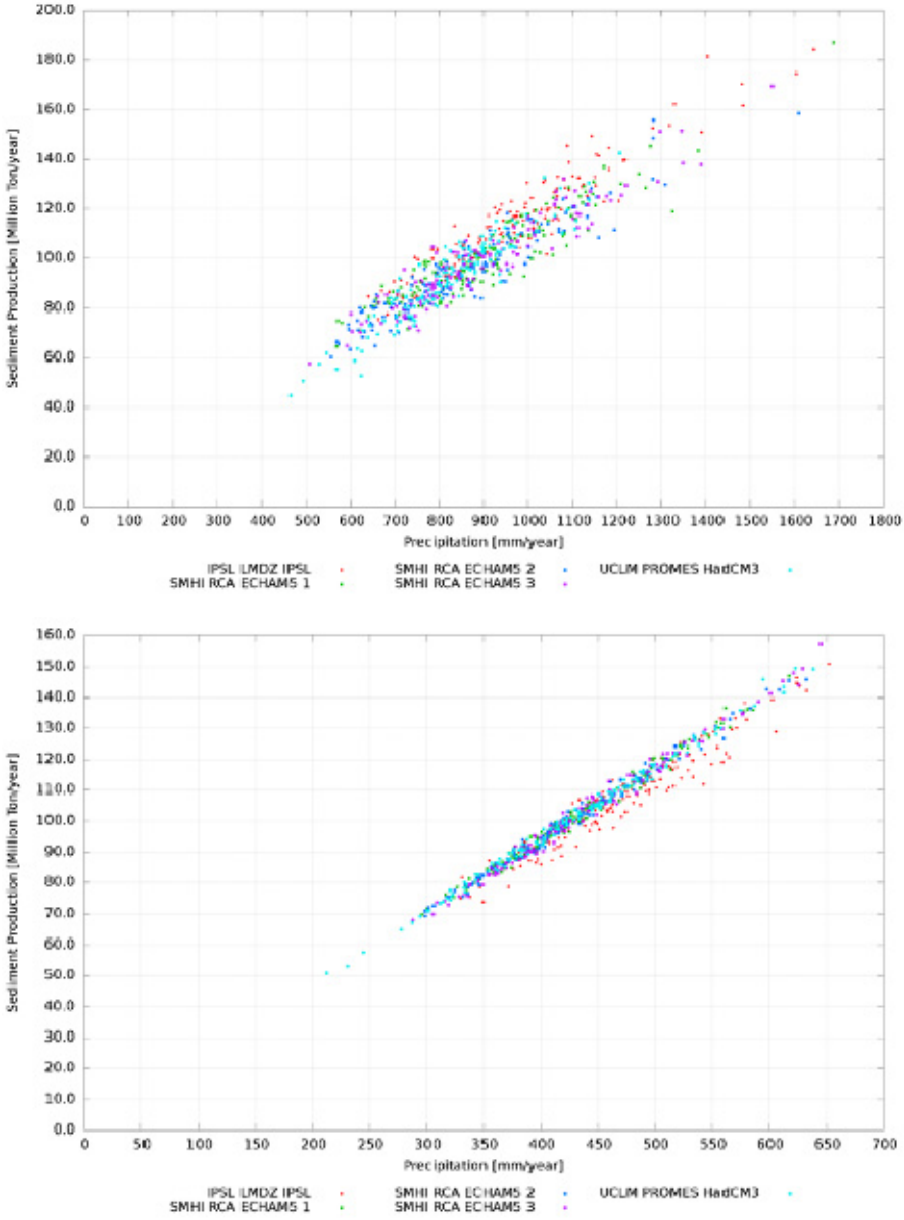

Figure 13. Correlation between annual sediment yield and mean annual precipitation: a) Bermejo Basin and b) Pilcomayo Basin.

To determine future scenarios for sediment transport in the Bermejo River, important in assessing the Parana Delta Front advancement, two types of evolutions were taken in account (Figure 14). For this, two envelope lines were drawn for sediment yield results in the Bermejo basin to estimate scenarios of wash load in the Parana Delta: one with a steady growth of 69,000 ton/year per year and another with a decrease of 48,000 ton/year per year. Those results were used for modeling the Parana Delta Front advancement.

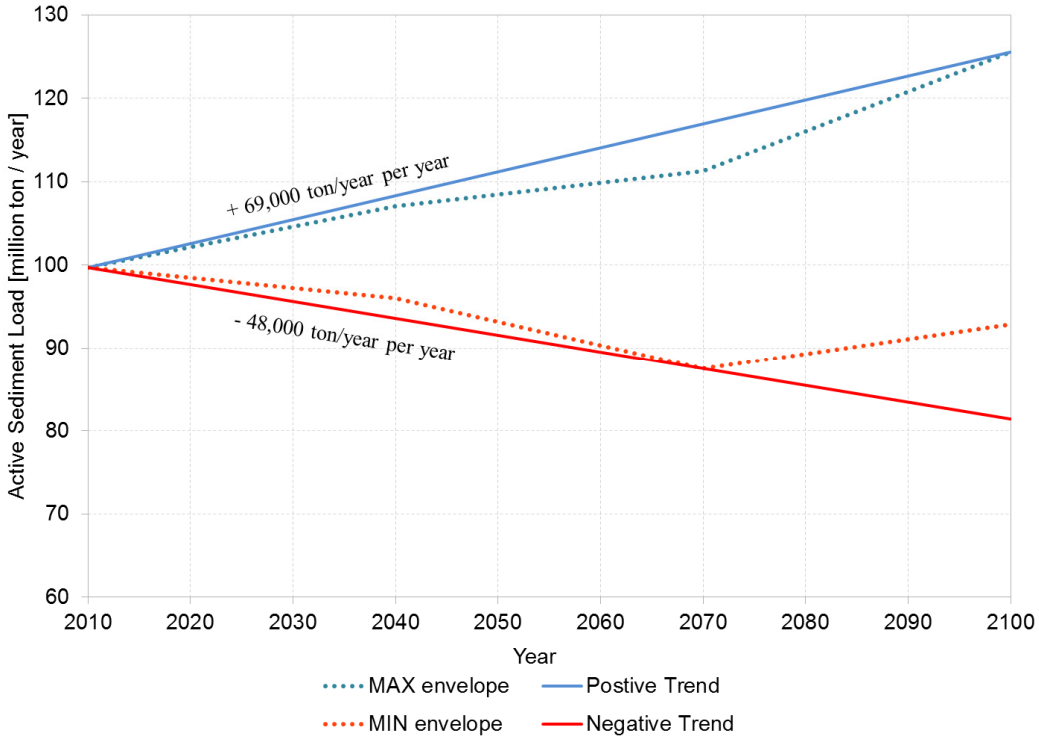

Figure 14. Evolution of sediment charge in Bermejo River.

Advance of the Paraná river Delta Front

Modeling Framework

Soil profiles of the Parana River Delta Front (Silva Busso et al., 2004; Rinaldi et al., 2006) indicate that the growth of the frontal area is produced by the deposition of fine sands and coarse silts (coarser sands deposit along the existing delta). Previous numerical studies have assumed that this sediment mixture can be treated as fine sediment (Sarubbi and Menéndez, 2007).

Following this approach, a sedimentological model for the suspended fraction was developed, which includes the advection, dispersion, deposition and resuspensión processes. This was driven by a 2D hydrodynamic model, which solves the set of Swallow Water Equations. Sediment concentrations are assumed to be constant in the vertical direction. For deposition and resuspension, simple shear stress models were adopted.

In order for medium and long term simulations to be possible, a simple morphological model was implemented, which computes the variation of the bottom elevation due to sediment deposition, producing a feedback loop between sediment and hydrodynamics.

To assure a strong coupling between all processes, these sub-models were integrated in a single code. This modeling framework is schematized in Figure 14.

Under the hypothesis that individual storm surges in the estuary have limited influence over the long term growth of the delta, only mean hydrodynamic conditions were simulated, using only astronomical tide variations and disregarding wind shear.

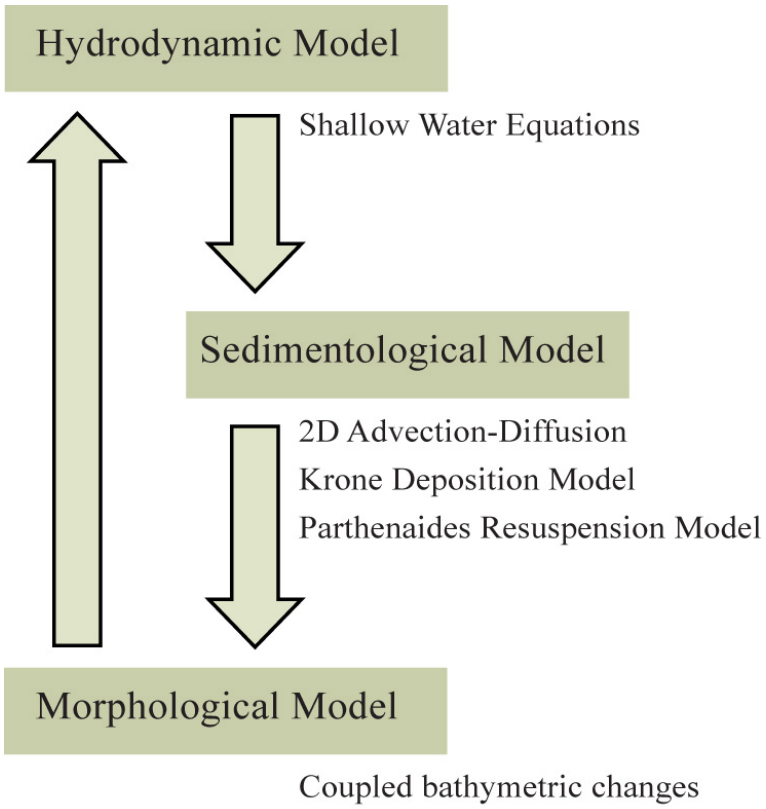

Figure 14. Modeling framework.

The set of Shallow Water Equations (*SWEs*) describe the dynamics of an incompressible fluid within a domain in which the depth of the flow is small compared to the horizontal dimensions of the problem. These can be derived by integrating the Navier-Stokes equations along the vertical direction under the assumption that vertical components of the velocity and acceleration are negligible and hence pressure distribution is hydrostatic.

The set of *SWEs* is composed of a scalar equation of mass conservation and two scalar equations of momentum conservation, one for each horizontal direction. These equations have been published many times under this form (Anastasiou and Chan, 1997). However, the modeling approach adopted in this work requires momentum conservation equations to be written in their vectorial form. *SWEs* then result:

$$\frac{\partial h}{\partial t} + \nabla \cdot \left(h\mathbf{U} \right) = 0 \qquad [8]$$

$$\frac{\partial}{\partial t}\left(h\mathbf{U}\right)+\nabla\cdot\left(h\mathbf{U}\mathbf{U}^{T}\right)-\nabla\cdot\left(\nu_{t}h\nabla\mathbf{U}\right)=-\left|\mathbf{g}\right|h\nabla\left(h+h_{0}\right)-\frac{\boldsymbol{\tau}^{b}}{\rho}-\mathbf{f}\times h\mathbf{U} \qquad [9]$$

where h = flow depth; $\mathbf{U}$ = flow velocity; $\boldsymbol{\tau}^{b}$ = bottom shear stress; ν_t = eddy viscosity; $\mathbf{f} = (2\boldsymbol{\Omega}\bullet\mathbf{g})\bullet\mathbf{g}$ = Coriolis coefficient ($\boldsymbol{\Omega}$ = earth angular velocity, $\mathbf{g}$ = gravity acceleration vector); ρ = water density; and h_0 = bottom level.

Conservation equations for the sediments were written, both for the suspended and the deposited fractions. The sediment in question, hereafter called active, are only those relevant for this problem, aggregating fine sands and coarse silts into a single uniform load. In tensorial notation, the suspended sediment mass conservation equation is:

$$\frac{\partial C}{\partial t}+\nabla\cdot\left(\frac{h\mathbf{U}}{h}\cdot C\right)-\nabla\cdot\left(K\nabla C\right)=-\frac{D}{h}+\frac{R}{h} \qquad [10]$$

where C = sediment concentration; K = dispersion coefficient; D = deposition rate; and R = resuspension rate.

The equation for mass conservation of deposited sediments is:

$$\frac{\partial B}{\partial t}=D-R \qquad [11]$$

where B = bottom sediment load [kg/m^2].

For the deposition and resuspension processes, common shear stress based formulation for fine sediments were adopted (Mehta and McAnally, 2008). Krone (1962) model was selected for the calculation of deposition rate:

$$D=\begin{cases} C\cdot W_{s}\cdot\left(1-\dfrac{\left|\boldsymbol{\tau}^{b}\right|}{\tau_{cr,d}^{b}}\right) & \text{si } \left|\boldsymbol{\tau}^{b}\right|<\tau_{cr,d}^{b} \\ 0 & \text{si } \left|\boldsymbol{\tau}^{b}\right|\geq\tau_{cr,d}^{b} \end{cases} \qquad [12]$$

where W_s = is the sediment fall velocity, function of the characteristic diameter; and $\tau^b_{cr,d}$ = critical shear stress for deposition, function of the type of sediment.

For the resuspension rate, Parthenaides (1962) model was adopted:

$$R = \begin{cases} E_0 \cdot \left(\dfrac{\left|\boldsymbol{\tau}^b\right|}{\tau^b_{cr,r}} - 1 \right) & \text{si } \left|\boldsymbol{\tau}^b\right| > \tau^b_{cr,r} \\ 0 & \text{si } \left|\boldsymbol{\tau}^b\right| \le \tau^b_{cr,r} \end{cases} \qquad [13]$$

where $\tau^b_{cr,r}$ = critical shear stress for resuspention; and E_0 = erodibility constant. While these parameters depend on the consolidation state of the deposited sediments, they were considered constant for the purpose of this work.

The morphologic submodel consists in updating the bottom level according to:

$$h_0 = h_0^0 + \frac{B \cdot \varphi}{\rho_s \cdot p} \qquad [14]$$

where h_0^0 = initial bottom level; ρ_s = sediment density; p = deposited sediment porosity, considered constant in time; and φ = 'acceleration factor'. The acceleration factor is an artifact to speed up the evolution of the bathymetry, allowing the reduction of computer time for long term runs. A value of 100 was used in this paper, as a very low sensitivity of the results was verified when comparing with results with a lower value.

For the development of the numerical model OpenFOAM (Field Operation and Manipulation; Weller et. al., 1998) was used. OpenFOAM is an open source toolkit for the development of customized numerical solvers for the solution of continuum mechanics problems, especially computational fluid dynamics (*CFD*). This toolkit includes a multitude of libraries, utilities and basic solvers which streamline the development of numerical models. OpenFOAM is based on the finite volume method. Its chief advantage comes from its novel design, which implements the object-oriented paradigm. In particular, discretized

differential equations are treated as objects which, through carefully designed operator overloading, are written in a way they closely resemble their analytical counterparts written in tensorial notation. This feature, along the implementation hiding typical of object-oriented programming, greatly increase code clarity and allow the developer to concentrate in the top level of the code.

Current numerical model is based on basic solver included in OpenFOAM (named *shallowWaterFoam*) for the solution of inviscid *SWEs*. In this solver both internal and bottom shear stresses are missing from Equation 9. The solver is based on the PISO method (Pressure Implicit with Splitting Operators; Issa, 1986) for time stepping. This method has an initial predictive stage in which the momentum equation is solved using the water levels from the previous time step. In a second corrective stage, the semi-discretized momentum equation is replaced in the continuity equation, which is solved for a new set of flow depths which verify continuity. This corrective stage can be iterated if necessary, updating the nonlinear terms of the equation.

For this work, the solver was modified to use conservative variables (h and $\mathbf{q} = h\mathbf{U}$, were $\mathbf{q}$ is specific discharge) to ensure conservation and simplify boundary conditions. The solver was then modified to introduce the viscous stresses. Bottom shear stress was modeled through the Chezy-Manning equation:

$$\boldsymbol{\tau}^b = -\rho \cdot |\mathbf{g}| \cdot \frac{\mathbf{q}}{h} \cdot \left|\frac{\mathbf{q}}{h}\right| / \frac{h^{2/6}}{n^2} \qquad [15]$$

where n = Manning coefficient. Picard's linearization was applied to the term previous to implicit discretization.

To allow at least a partially implicit discretization of the internal turbulent tensions, the diffusive term of Equation 9 was rewritten as:

$$-\nabla \cdot \left(\nu_t h \nabla \mathbf{U}\right) = -\nabla \cdot \left(\nu_t \nabla \mathbf{q}\right) - \nabla \cdot \left(\nu_t \left(h \nabla U - \nabla \mathbf{q}\right)\right) \qquad [16]$$

allowing the first term to be evaluated implicitly while the second term, which is smaller, was discretized explicitly.

For the eddy viscosity coefficient a constant value was adopted throughout the modeling domain.

During the simulation, as a result of sediment deposition, certain cells near the cost would become dry during low tide. To enable the model to handle this situation without introducing instabilities, a simple algorithm was introduced. It consists on modifying the bottom elevation of those cells after each time step, lowering the cell, if necessary, to ensure that a minimum depth (20 cm was adopted) is maintained at all time. When the water level rises, the bottom level is gradually restored to its correct level. With this treatment, any cell with a water depth equal to the minimum depth is considered as dry from the standpoint of calculating the advance of the delta front.

While this simple algorithm does not rigorously ensure mass conservation, the dry portion of the domain is relatively very small, so the associated error is not significant. Additionally, the amount of water that can flow through these minimum depth cells is almost negligible, so they effectively behave as dry contours from the hydrodynamic point of view. This approach is considered to be accurate enough given the objectives of the present work.

The implementation of the two differential equations governing the sediments dynamics using OpenFOAM was relatively straightforward. They are solved within the main loop for each time step once the hydrodynamic equations have been solved.

Resuspension flux was calculated for each time step explicitly wherever deposited sediments were available. Deposition flux was calculated implicitly while solving the equation for conservation suspended sediments.

Finally, the morphological equation is solved explicitly and the bottom elevations are updated.

A verification of the hydrodynamical model, with special emphasis on the viscous terms introduced to the basic OpenFOAM solver, was performed by comparing results with a well-established shallow water code, HIDROBID II (Menéndez, 1990), for a simple test case.

The test used for comparison is a channel flow of geophysical scale with an abrupt expansion and flat bottom. The dimension of the modeling domain is presented in Figure 15a. The calculation mesh is made

of quadrilateral cells of 100m of size. For the left side, an inflow boundary condition of 15,000 m^3/s was used, while a constant depth of 5m was specified for the right boundary. For both models, constant eddy viscosity of 100 m^2/s and Manning coefficient of 0.015 were specified. The models were run to steady state and specific discharge magnitudes were compared. These are presented in Figures 15b and 15c for HIDROBID II and the current model respectively. A close match is observed.

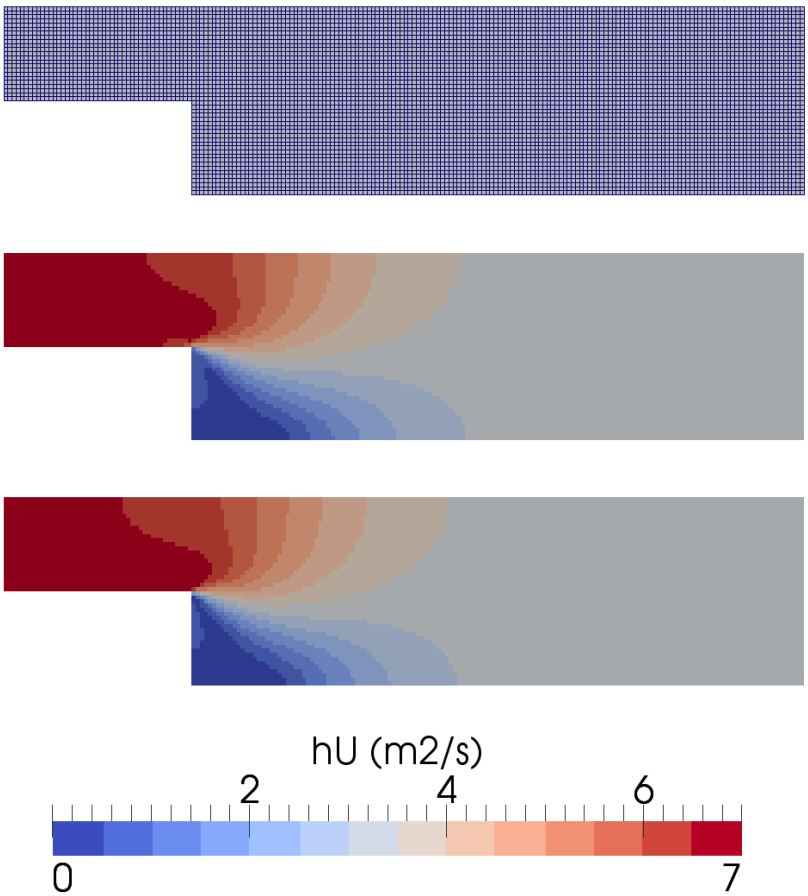

Figure 15. Hydrodynamic validation case (a); HIDROBID II results (b); current model results (c).

Parana River Delta Front Model

The model outlined in section 2 was applied to the simulation of the Parana River Delta Front. The simulation domain includes the region known as Upper Plata River (Figure 16), extending 60 km in the

east-west direction and 110 km in the north-south direction, with an area of 3300 km^2. The Upper section of the Plata River extends to the line joining the cities of La Plata (Argentina) and Colonia (Uruguay). The system is mainly forced by the liquid and solid discharges of the tributary discharging to the Plata River and the tidal wave propagating from the Atlantic Ocean.

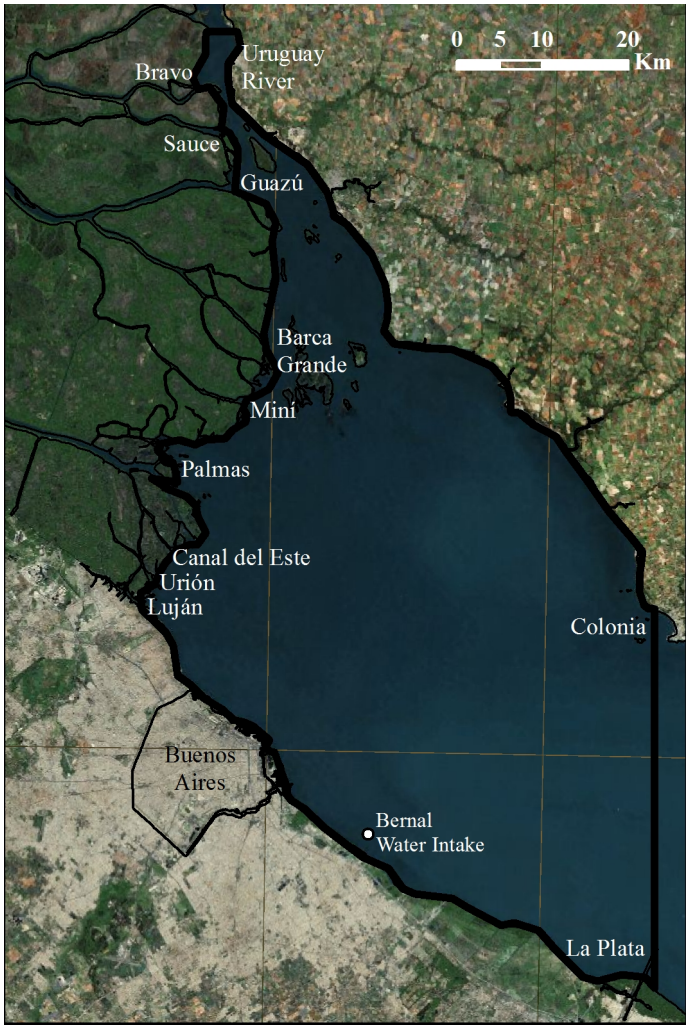

Figure 16. Simulation domain and tributaries

Only mean conditions were simulated; hence only astronomical tidal waves were introduced in the downstream side of the domain. This boundary was implemented as a fixed water level condition, constructed by interpolating astronomical tide time series from La Plata and Colonia cities.

The main source of liquid and solid discharge to the system is the Parana River. The input discharge was divided between eight branches of the Parana River (Table 2), totaling 17,000 m^3/s and 24 million ton/year of active sediments. The flow partition among the branches was made following the work of Bombardelli et al. (1995). The active sediment load for the Parana River (i.e., the part of the suspended load involved in the Delta growth process) was introduced as a constant concentration, equal for every branch. The introduction of all the branches of the Parana as inflow boundary conditions, even those with relatively low discharge, played a key role by making sediment available for deposition in the areas in which growth is observed. This is consistent with Syvitski et al. (2005).

Liquid discharges were also introduced for the Uruguay and Lujan Rivers. These discharges are located at the eastern and western extremes of the delta front respectively, shielding the coast of Uruguay and Buenos Aires from the sediments transported by the Parana. Neither of these rivers transports any appreciable active sediments.

A semidiurnal oscillation was introduced for the discharge of every tributary. This is produced by the astronomical tide. A semi-amplitude of 50% the mean discharge was estimated for the Parana and Uruguay Rivers, while 500% was adopted for the Lujan River, for which current measurement exist near the mouth.

Table 2. Combination of RCM and GCM.

River Branch	Liquid discharge (m^3/s)	Sediment concentration (m^3/s)
Parana Bravo (Parana)	3600	0.045
Sauce (Parana)	3600	0.045
Parana Guazu (Parana)	4359	0.045
Barca Grande (Parana)	1060	0.045
Parana Mini (Parana)	471	0.045
Canal del Este (Parana)	78	0.045
Urion (Parana)	78	0.045
Uruguay	4622	-
Luján	15	-

For the calculation of the deposition rate, the fall velocity was calculated using van Rijn (1984) formulation, with a mean grain size for the sediments (d50) of 0.15 mm. This size is representative of the

active fraction of fine sands and coarse silts responsible of the delta growth. Van Rijn formulation yields a fall velocity of 0.02 m/s.

In previous sedimentologic models of the Inner Plata River (FIUBA, 1999; Menéndez and Castellano, 2000a, b; Menéndez, 2001; Sarubbi and Menéndez, 2007), which comprises the Upper section, the critical shear stresses for deposition and resuspension were based on the work by Harrison & Owen (1971). For this work, those values were used as a starting point and were subsequently adjusted slightly by calibration, finally adopting 0.1 N/m^2 and 0.15 N/m^2 for the critical stresses for deposition and resuspension, respectively.

The erodibility coefficient has a broad uncertainty range (Krestenitis et al., 2006). For this work, a value of 2×10^{-5} $kgm^{-2}s^{-1}$ was adopted.

The calculation mesh was generated using GMSH software (Geuzaine and Remacle, 2009). It is composed of 106,000 triangular cells, with a minimum size of 100m near the delta front, and a maximum size of 1000m (Figure 17). For stability, the time step was fixed at 5 s, insuring a maximum Courant number of around 0.5.

Both for the eddy viscosity and the dispersion coefficient, a constant value of 40 m^2/s was adopted.

For the Manning coefficient a value of 0.02 was adopted. The sediment density was taken as 2650 kg/m^3, and a porosity equal to 0.4 was considered.

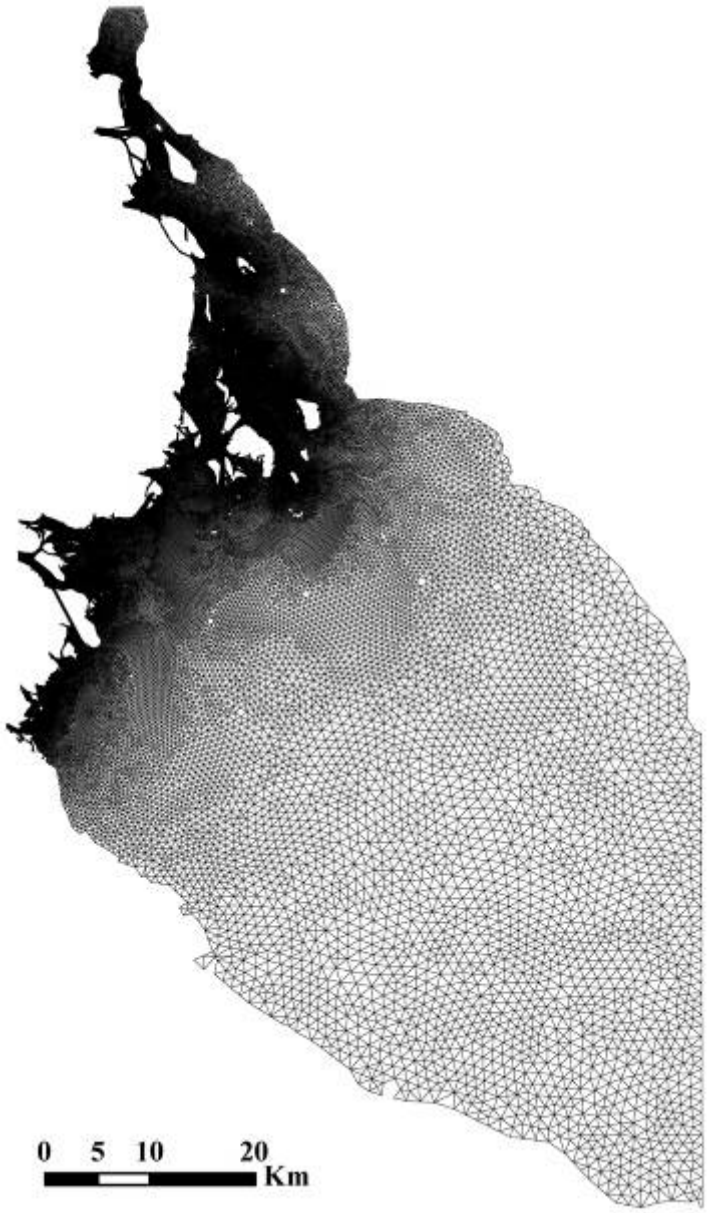

Figure 17. Calculation mesh

In order to calibrate the numerical model and assess its ability to correctly simulate the advance of the delta front, a simulation of the 1994-2007 period was performed. For both these years nautical charts exist, published by the Naval Hydrographic Service of Argentina. These charts contain not only coastlines for the delta front (which match satellite images for those periods), but also bathymetric data. The mesh and initial bathymetry were constructed based on the 1994 data.

The simulation of mean conditions was performed for the specified period, starting from a stabilized hydrodynamic condition. The advance of the delta front was calculated for the final year of the

simulation and compared to the recorded coast line. This comparison is presented in Figure 18. The overall agreement is considered as satisfactory.

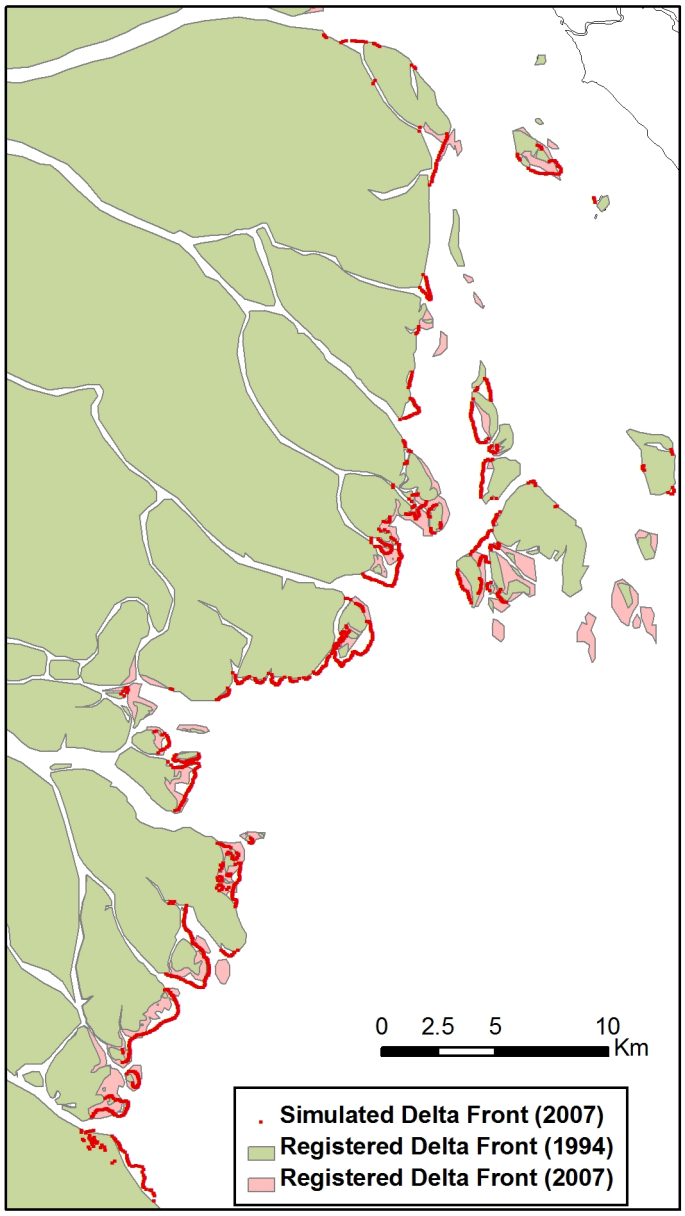

Figure 18. Comparison of recorded and simulated advance of the Delta Front for the 1994-2007 period.

Current velocity measurements at Bernal water intake (Figure 5) for a period during which there was a moderate wind situation were available. The comparison with simulated results (Figure 19) shows that the direction and magnitude of currents are consistent with measurements, although measurements show a larger dispersion.

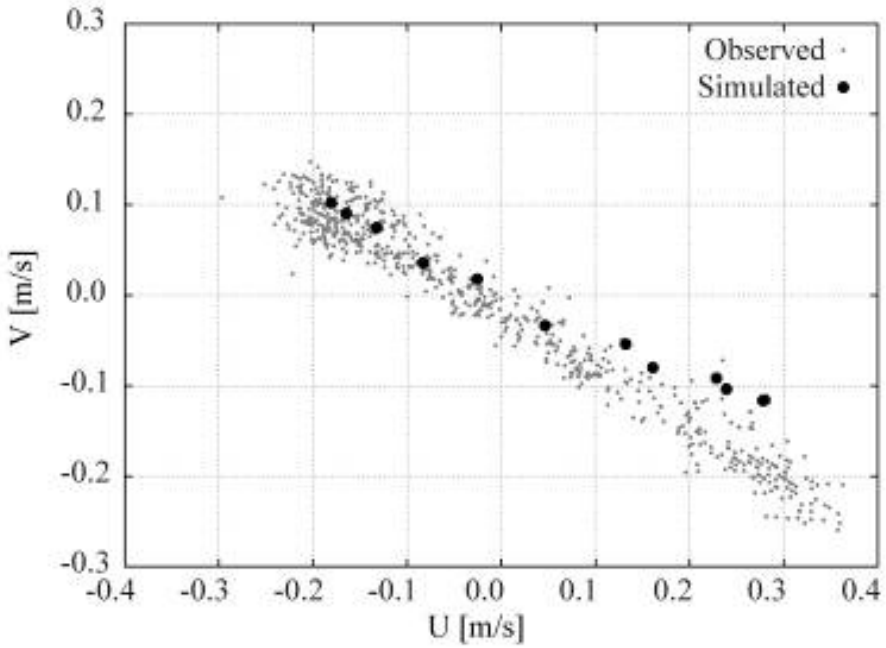

Figure 19. Current comparison at Bernal water intake

Future Scenarios

Long term simulations were performed with the calibrated numerical model. These simulations allow the prediction of the growth of the Parana River Delta Front for the next few decades.

In the first place, a base simulation was performed for the 2007-2040 period maintaining the same parameters and discharges values as in the calibration run. This established a baseline for the assessment of the system behavior under the effects of climate change. The resulting delta frontline for 2007, 2020 and 2040 is presented in Figure 20. The simulation indicates that higher rates of growth should be expected for two zones: between the Miní and Palmas branches, and between Canal del Este and Urion branches.

In Figure 21 the time series of the Delta Front area growth for this baseline scenario is presented. The mean area growth is about 1.6 km^2/year.

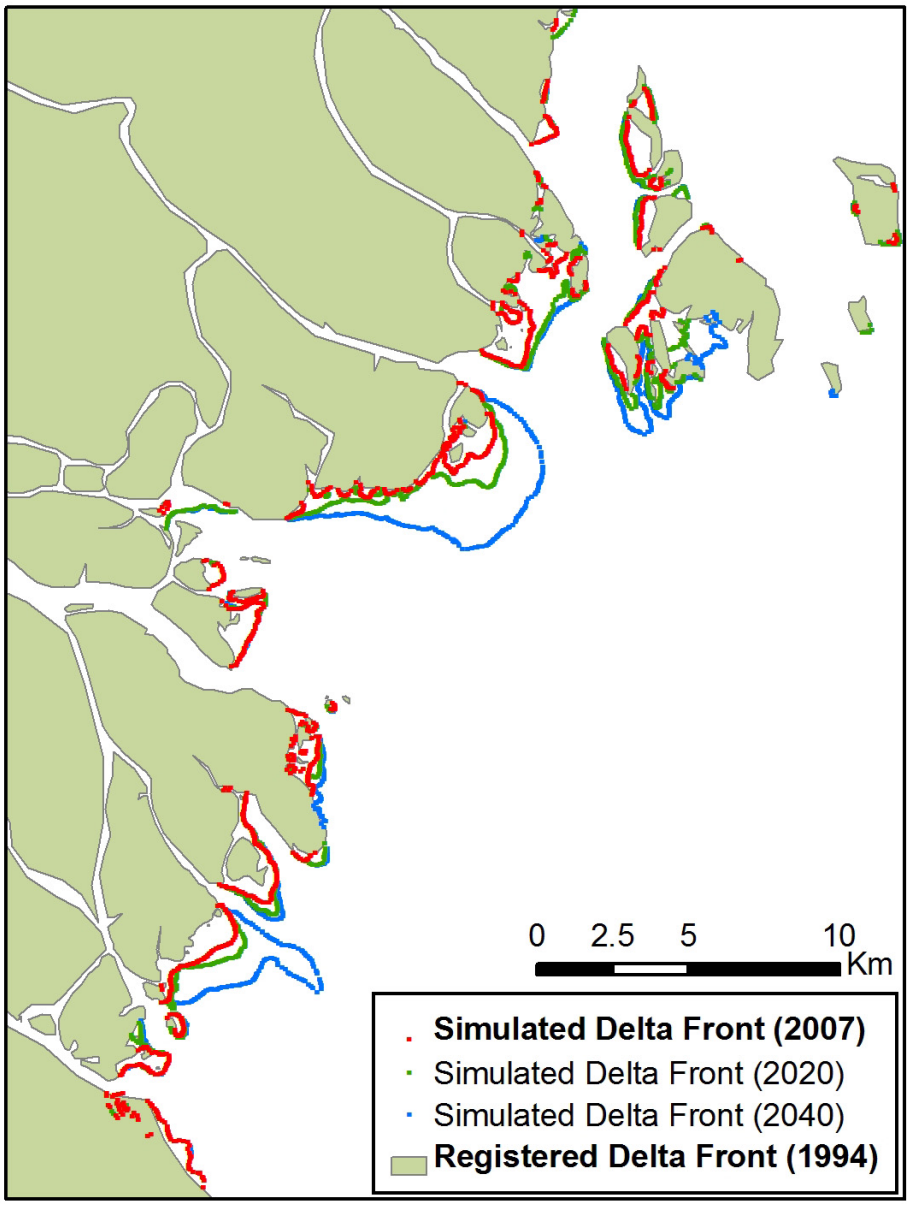

Figure 20. Simulated Delta Front for the base condition 2007-2020-2040.

Climate change scenarios were defined next. To better understand the individual impact of each variable, tests were performed by changing them independently. In the first place, a sea level rise at a constant rate of 1.7 mm/year was tested. In the second place, the active sediment load was varied according to Figure 13.

The resulting area growth time series for each scenario are presented in Figure 21, while the corresponding frontlines for 2040 are shown in Figure 22. Note the significant decrease of the area

growth for the mean sea level increase scenario. This is consistent with the classification of the Parana River Delta as under 'great risk' due to sea level rise, performed by Syvitski (2009).

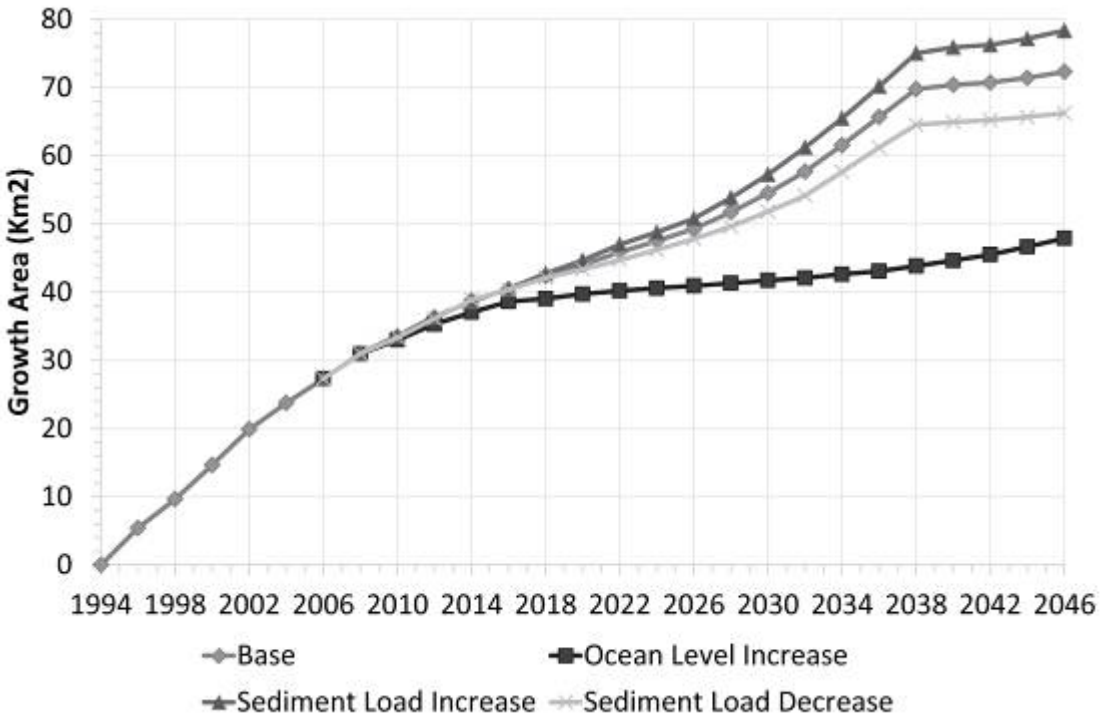

Figure 21. Delta area growth for different scenarios

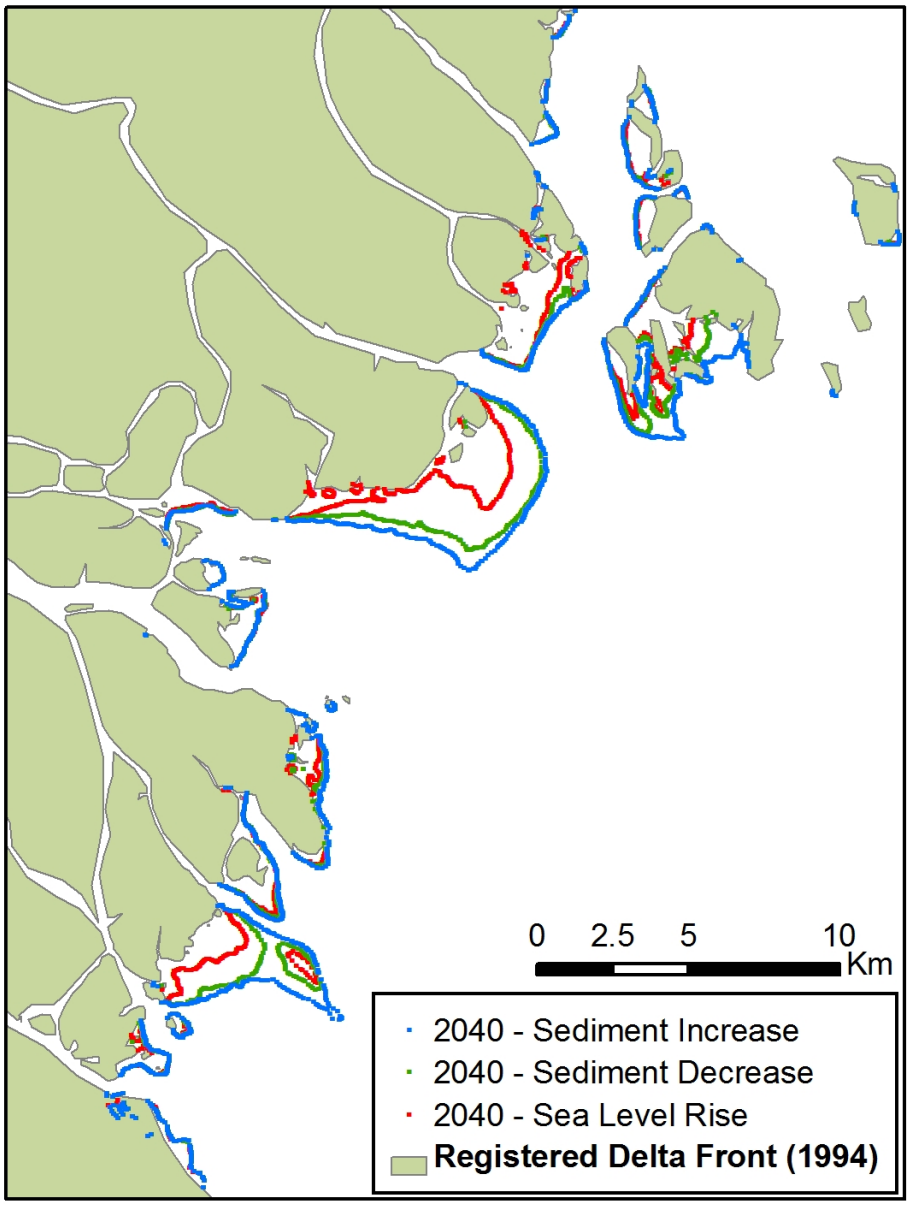

Figure 22. Simulated Delta Front for 2040 Scenarios

The results for future climate change scenarios show that mean sea level rise is a key factor in reducing the area growth rate. The effect of variations in sediment load is less significant. Sensitivity to changes in liquid discharge remains to be tested.

References

Aceituno, P., Elementos del Clima en el Altiplano Sudamericano, Revista geofísica 44, pp. 37-55 Enero-Julio, 2006.

Alarcón, JJ., Szupiany, R., Montagnini, M.D., Gaudin, H., Prendes, H.H. y Amsler, M.L. (2003): "Evaluación del Transporte de Sedimentos en el Tramo Medio del río Paraná", Primer Simposio Regional sobre Hidráulica de Ríos, Ezeiza.

Amsler ML, Drago E.C.E. (2007): A review of suspended sediment budget at the confluence of the Paraná and Paraguay Rivers, Hydrolog Process (in press).

Anastasiou, K., Chan, C.T., Solution of the 2D shallow water equations using finite volume method on unstructured triangular meshes. Int. Journal for Numerical Methods in Fluids, Vol. 24, 1225-1245, 1997.

Bombardelli, F.A., Menéndez, A.N., Brea, J.D., Lapetina, M.R., y Uriburu Quirno, M., Estudio hidrodinámico del Delta del río Paraná mediante modelación matemática. Informe LHA-INCyTH 137-03-95, 1995.

Brea, J.D., Spalletti P., Busquets M., 1999; Generación y transporte de sedimentos en la Alta Cuenca del Río Bermejo. Impacto en el Sistema Paraguay-Paraná-Río de la Plata, y el Delta del Paraná. Programa Estratégico de Acción para el Desarrollo Sustentable de la Cuenca del Río Bermejo, Fondo para el Medio Ambiente Mundial - FMAM (Global Environmental Fund - GEF), OEA. Instituto Nacional del Agua y del Ambiente – Laboratorio de Hidráulica y del Ambiente, Informe LHA 177-04-99.

Brea, J. D., Spalletti, P., Avances, Retrocesos y Estancamientos sobre el Conocimiento de los Procesos Fluviales del Río Pilcomayo, Quinto Simposio Regional sobre Hidráulica de Ríos, Santiago del Estero, 2-4 of November, 2011.

Campetella C.M, Possia, N.E., Upper-level cut-off lows in southern South America. Meteorology and Atmospheric Physics, v. 96, pp. 181- 191, 2007.

FIUBA, Estudio del impacto ambiental sedimentológico de las pilas del puente principal de la conexión Buenos Aires - Colonia. Informe Ejecutivo. Agosto 1998.

Garreaud, R.D., Aceituno, P., Interannual Rainfall Variability over the South American Altiplano, Journal of Cliamte, vol. 14, pp. 2779-2789, June, 2001.

Gavrilovic, Z., (1988). The use of an empirical method (erosion potential method) for calculating sediment production and transportation in unstudied or torrential streams. International conference of river regime, 18-20 May, Wallingford, England, 411-422.

Geuzaine C.,Remacle, J-F. Gmsh: a three-dimensional finite element mesh generator with built-in pre- and post-processing facilities. International Journal for Numerical Methods in Engineering, Volume 79, Issue 11, pages 1309-1331, 2009.

Globevnik, L.; Holjevik, D.; Petkovsek, G.; Rubinic, J., (2003). Applicability of the Gavrilovic method in erosion calculation using spatial data manipulation techniques. In: De Boer, D.; Froehlich, W.; Mizuyama, T.; Pietroniro, A. (Eds.). Erosion prediction in Ungauged Basins: Integrating methods and techniques, 279. IAHS Publication, 22-233.

González M.H. and Murgida A.M., Seasonal Summer Rainfall Prediction in Bermejo River Basin in Argentina, Climate Variability - Some Aspects, Challenges and Prospects, Dr. Abdel Hannachi (Ed.), pp. 141-160, 2012.

Harrison, A.J.M., Owen, M.W., Siltation of fine sediments in estuaries. IAHR XIV Congress, 1971.

Issa, R.I., Solution of the implicitly discretized fluid flow equations by operator-splitting. Journal of Computational Physics, 62(1):40-65, January 1986.

Irigoyen, M.A., Spalletti, P., Brea, J.D., Uso de Imágenes para Caracterizar la Cobertura Vegetal en la Producción de Sedimentos, Quinto Simposio Regional sobre Hidráulica de Ríos, Santiago del Estero, 2-4 of November, 2011.

Krestenitis, Y.N., Kombiadou, K.D., y Savvidis, Y.G., Modelling cohesive sediment transport in the marine environment: The case of Thermaikos Gulf. J. Ocean Sci. Disc., 3, 701–733, 2006.

Krone, R.B., Flume studies of the transport of sediment in estuarial shoaling processes. Hydraulic Engineering Laboratory, University of California, Berkeley, 1962.

Mehta, A.J., McAnally, W. H., Fine-Grained Sediment Transport. Sedimentation Engineering, American Society of Civil Engineers: American Society of Civil Engineers Manual 110, Chapter 4. 2008.

Menéndez, A.N., Sistema HIDROBID II para simular corrientes en cuencos. Revista internacional de métodos numéricos para cálculo y diseño en ingeniería, vol. 6, 1, 25-36, 1990.

Menéndez, A.N., Castellano, R., Simulation of sedimentation in an estuary due to an artificial island. 4th International Conference HydroInformatics 2000, Cedar Rapids, Iowa, USA, July, 2000a.

Menéndez, A. N., Castellano, R., Simulación numérica de problemas con escalas temporales disímiles: crecimiento de una barra de sedimentación. XI Congreso sobre Métodos Numéricos y sus Aplicaciones. ENIEF'2000, Bariloche, Noviembre, 2000b.

Menéndez, A.N., Description and modeling of the hydrosedimentologic mechanisms in the Rio de la Plata River. VII International Seminar on Recent Advances in Fluid Mechanics, Physics of Fluids and Associated Complex Systems, Buenos Aires, Argentina, 2001.

Partheniades, E., A study of erosion and deposition of cohesive soils in salt water. Ph.D. Thesis. University of California, Berkeley, 1962.

Peviani M.A., M. Baldin and L. Crepaldi (1994). Application of a sediment yield model to an east alpine basin.Man and Mountain '94. Ponte di Legno. Italia.

Re, M., Menéndez, A.N. and Amsler, M.L., 2009. Metología para la generación de series temporales de descarga sólida de los ríos Parana de las Palmas y Parana Guazu. RIOS 2009, Cuarto Simposio Regional sobre Hidráulica de Ríos. Salta, Argentina.

Rinaldi, V., Abril, E., y Clariá, J., Aspectos Geotécnicos Fundamentales de las Formaciones del Delta del Río Paraná y del Estuario del Río de la Plata. Revista Internacional de Desastres Naturales, Accidentes e Infraestructura Civil. Vol. 6(2), 2006.

Sarubbi, A., y Menéndez, A.N., Un modelo numérico para representar el avance del Frente del Delta del río Paraná a escala secular. Mecánica Computacional Vol XXVI, pp. 2203-2216, S.A. Elaskar, E.A. Pilotta, G.A. Torres (Eds.), Córdoba, Argentina, 2007.

Silva Busso, A., Amato, S., Seoane N., Pittau, M. G., Aportes al conocimiento de la geología del Delta del Río Paraná. Informe INA 03-235-04, Septiembre, 2004.

Spalletti, P.D., Brea, J.D., 2006. Efecto de cambios de la cobertura vegetal en la producción de sedimentos. Caso de la Alta Cuenca del río Bermejo. III Congreso Iberoamericano sobre Control de la Erosión y los Sedimentos (CICES 2006). Buenos Aires, Argentina, 9-11 de agosto.

Syvitski, J.P.M., Kettner A.J., Correggiari, A., Nelson, B.W., Distributary channels and their impact on sediment dispersal. Marine Geology 222–223, pp. 75–94, 2005.

Syvitski, J.P.M., Kettner A.J., Overeem I., Hutton E.W.H., Hannon M.T., Brakenridge G.R., Day J., Vörösmarty C., Saito Y., Giosan L. and Nicholls R.J., Sinking deltas due to human activities. Nature Geoscience 2, 681 – 686, 2009.

van Rijn, L.C., Sediment Transport, Part II: Suspended load transport. Journal of Hydraulic Engineering, ASCE, no 11, 1984.

Vera, C., W. Higgins, J., Amador, T., Ambrizzi, R., Garreaud, D., Gochis, D., Gutzler, D., Lettenmaier, J., Marengo, C. R., Mechoso, J., Nogues-Paegle, P. L., Silva Dias, y C. Zhang, A Unified View of the American Monsoon Systems. J. Climate, Vol. 19, 4977–5000, 2006.

Weller, H.G., Tabor, G., Jasak, H., Fureby, C., A tensorial approach to computational continuum mechanics using object orientated techniques. Computers in Physics, 12(6):620 - 631, 1998.

Zemlijc M., 1971; Calcul du debit solide - Evaluation de la vegetation comme un des facteurs antierosif. International Symposium Interpraevent, Villach, Austria.